

ON THE INITIALIZATION OF TYPICAL IGNITION MODELS IN THE CONTEXT OF SPARK-IGNITION DEVICES

Joaquín Aranciaga^a, Ezequiel J. López^a and Norberto M. Nigro^b

^a*Instituto de Investigación en Tecnologías y Ciencias de la Ingeniería, Universidad Nacional del Comahue-CONICET, Buenos Aires 1400, 8300 Neuquén, Argentina
joaquin.aranciaga@gmail.com, ezequiel.lopez@fain.uncoma.edu.ar*

^b*Centro de Investigación en Métodos Computacionales, Universidad Nacional del Litoral-CONICET, Predio CONICET “Dr. Alberto Cassano”, Colectora RN 168 s/n – Paraje El Pozo, 3000 Santa Fe, Argentina
norberto.nigro@cimec.santafe-conicet.gov.ar*

Keywords: Computational Fluid Dynamics, Premixed Combustion, Ignition, Spark Discharge

Abstract. Several ignition models have been proposed over the years in order to handle the complex phenomena taking place between the instant a spark is discharged in a combustible mixture and the arising flame becomes self-sustained. Energy stored either in an inductor or a capacitor flows from the primary to the secondary side of a transformer, where voltage becomes high enough to produce the breakdown of the gas. After the conducting channel is generated, energy is transferred either in arc or glow mode, depending on the electrical circuit parameters. Due to the extremely short time and length scales involved in the post-breakdown stage, it has become quite standard to employ the simplification of imposing an expanded hot plasma channel, whose thermodynamic state and dimensions depend on a few predominant parameters. As the temperature gradient is initially very high, a heat diffusion equation is normally solved to predict the plasma expansion until the temperature drops below a predefined threshold, such that heat diffusion effects are overcome by the chemistry of the mixture. In this work we assess the appropriateness of the usual approach and compare it to a more recent published alternative, both of which are meticulously analyzed. Main advantages and disadvantages of their utilization are underlined, and the need for a better approach is introduced.

1 INTRODUCTION

Over the last decades a growing number of research articles have been devoted to modeling spark-ignition events in combustible mixtures. In the field of safety engineering and process industry the goal is to predict the conditions at which an electric discharge may occur, and the associated energy (specifically the Minimum Ignition Energy, MIE) it must possess to start combustion reactions able to generate a fire and/or explosion. Among others, [Nakaya et al. \(2011\)](#), [Bane et al. \(2015\)](#) and [Essmann et al. \(2016\)](#) have performed numerical simulations around these low energy levels. On the other hand, simulations for spark-ignition engines (c.f. [Herweg and Maly \(1992\)](#); [Shen et al. \(1994\)](#); [Song and Sunwoo \(2000\)](#); [Colin and Truffin \(2011\)](#); [Lucchini et al. \(2013\)](#); [Sforza et al. \(2017\)](#)) entail somewhat different conditions, e.g., turbulent flows, higher discharged energies and different ignition system components leading to diverse voltage and current waveforms. For all these cases a transient combustion problem is to be solved for which an initial condition has to be adopted. The simplest initialization strategy consists in ignoring the extremely short breakdown stage and setting a presumed burnt gas volume, as done for example by [Tan and Reitz \(2006\)](#). Although reasonable results may be attained by following this procedure in particular cases, it is perceived as too simplistic to represent a whole range of ignition events. In fact, energy released during breakdown plays no role in kernel size or temperature determination for this approach, contradicting the importance given to this energy discharge mode by [Maly \(1984\)](#). One step further, the initial kernel size might be calculated in coherence with the critical energy definition which depends on the laminar flame thickness, as done by [Colin and Truffin \(2011\)](#). In this case, a higher breakdown energy mildly reduces the time of the burnt kernel insertion into the domain. A much more common methodology (c.f. [Shen et al. \(1994\)](#); [Song and Sunwoo \(2000\)](#); [Falfari and Bianchi \(2007\)](#); [Forte et al. \(2010\)](#); [Lucchini et al. \(2013\)](#); [Cornolti \(2015\)](#); [Zhu et al. \(2016\)](#); [Sforza et al. \(2017\)](#)) follows the ideas presented by [Refael and Sher \(1985\)](#). In that paper the plasma channel diameter and temperature after breakdown are computed following a two-stage model (to be referred as TSM for the rest of the present work): an isochoric energy addition (breakdown energy) and a subsequent expansion to the chamber pressure at constant mass. Recently, [Meyer and Wimmer \(2018\)](#) exposed an apparently strong deficiency of TSM, namely the remarkable high temperatures after channel expansion, which was notably improved by their simple zero-dimensional thermodynamic model (ODTM). The main objective of the present article is to assess the appropriateness of both methodologies, considering their advantages and disadvantages, and appraise the necessity of further development. To this end, computational simulations are performed to serve as a basis of comparison for kernel temperatures and geometries. Firstly, TSM, iTSM (an improved variant of TSM) and ODTM are analyzed. Subsequently, the set of differential equations to be solved and the solution strategy are introduced. The simulation cases are described afterwards. Finally, relevant computational results are shown and main conclusions are drawn.

2 IGNITION MODEL ANALYSIS

2.1 TSM

In this model, the breakdown energy (E_{bd}) is added to a cylindrical volume whose radius directly depends on this energy, the unburned gas temperature (T_u) and pressure (p_0) and presumed peak temperature after the first (isochoric) stage ($T_{bd} \approx 60000$ K, according to [Maly \(1984\)](#)). The resulting low volume, high pressure channel expands afterwards as a closed system against the pressure outside of it, which is p_0 . Assuming an ideal gas with constant properties, the temperature (T_i) and diameter (d_i) of the plasma channel after expansion are given

by:

$$T_i = T_u \left[\frac{1}{\gamma} \left(\frac{T_{bd}}{T_u} - 1 \right) + 1 \right] \quad (1)$$

$$d_i = 2 \left[\frac{\gamma - 1}{\gamma} \frac{E_{bd}}{\pi d_g p_0 \left(1 - \frac{T_u}{T_i} \right)} \right]^{0.5} \quad (2)$$

where d_g is the spark gap and γ the specific heat ratio. As γ for a thermal plasma was not specified, every group of authors who employed this model assumed a different value. Shen et al. (1994), Song and Sunwoo (2000), Falfari and Bianchi (2007) and Forte et al. (2010) gave no specification about it. Lucchini et al. (2013) used the value corresponding to the unburned mixture, Cornolti (2015) estimated it using the average temperature between T_i and T_{bd} , while Sforza et al. (2017) followed Zhu et al. (2016) setting a value of 1.66, considering the plasma channel as a monoatomic gas. Due to its popularity, it is worth to determine a correct value of γ such that the idea behind the model is preserved. This is done next.

2.2 iTSM

An evident oversimplification of TSM is the assumption of an ideal gas with constant properties, considering the changes in composition, temperature and pressure the plasma is subjected to. Sher et al. (1992) elaborated on the original model by following the same two-step process, this time computing the thermodynamic plasma properties including dissociation, ionization and the different molecular energy storage modes, and transport properties evaluated from molecular theory, accounting for ionization. This version of the model will be termed iTSM (for improved Two-Stage Model). As no analytical solution exists for the post-expanded channel temperature and diameter, only graphical results were shown in the reference. In the spirit of determining the appropriate value of γ in TSM, computations are first carried out using thermodynamic and transport properties in equilibrium air plasmas provided by D'angola et al. (2008). Given the initial air state, the end of the first step (isochoric heat addition) is obtained by the application of energy conservation:

$$\rho_1 V_0 u_1 = \rho_0 V_0 u_0 + E_{bd} \quad (3)$$

$$\rho_1 = \rho_0 \quad (4)$$

where ρ , V and u are density, volume and specific internal energy, respectively, and subscript 0 (1) refers to the initial (final) state. As one will normally fix the maximum temperature, and considering that both ρ and u depend on temperature and pressure, the problem consists in finding the pressure that enforces Eq. (4), and afterwards solving Eq. (3) to obtain the initial plasma diameter. Then, this high pressure plasma channel is expanded to the chamber pressure at constant mass:

$$\rho_1 V_0 u_1 = \rho_i V_i u_i + p_0 (V_i - V_1) \quad (5)$$

$$\rho_2 V_i = \rho_1 V_0 \quad (6)$$

where subscript i refers to the post-expanded state, whose temperature and diameter are found by an iterative procedure. Computations obtained by this process correspond to iTSM. These

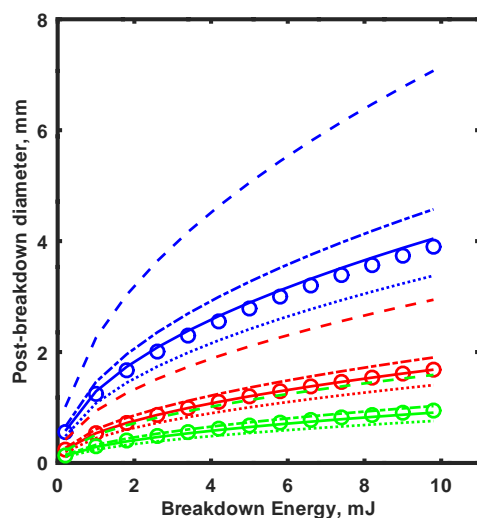


Figure 1: Post-breakdown diameters vs. breakdown energy. Symbols: iTSM. Lines: TSM. Blue, red and green indicate different unburned temperature ($T = 300, 450, 600$ K) and pressure ($p = 1, 5.8, 20$ bar), respectively. Dotted, full, dash-dotted and dashed lines stand for $\gamma = 1.1, 1.15, 1.2, 1.66$, respectively.

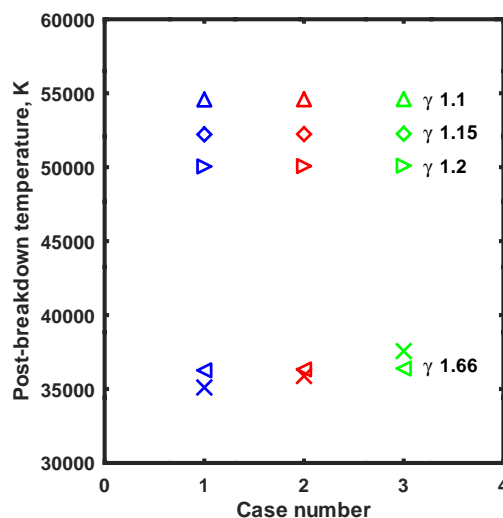


Figure 2: Post-breakdown temperatures. Crosses: iTSM. Other symbols: TSM results for different γ . Blue, red and green indicate different unburned temperature ($T = 300, 450, 600$ K) and pressure ($p = 1, 5.8, 20$ bar), respectively.

have been contrasted with the graphical information provided by [Sher et al. \(1992\)](#) and agreed very well, despite having resorted to different thermodynamic and transport properties.

Figure 1 depicts the post-breakdown diameter as a function of breakdown energy for three different unburned mixture states: 300 K - 1 bar (blue), 450 K - 5.8 bar (red) and 600 K - 20 bar (green). Symbols reflect predictions of iTSM, while lines represent the output of TSM for different values of γ (specified in the caption). The best agreement is achieved with $\gamma = 1.15$ for the three initial conditions assessed. Figure 2 shows the post-breakdown temperature as a function of breakdown energy for the same three initial states. Crosses mark the output of iTSM, while other symbols correspond to different γ of TSM. Based on temperature one would select $\gamma = 1.66$, as adopted by [Sforza et al. \(2017\)](#) and [Zhu et al. \(2016\)](#), but the error in the expanded channel diameter is too high, according to Fig. 1. This error diminishes with increasing pressures, but nonetheless remains consequential even for the highest pressure tested. As clearly seen, no single γ is capable of delivering both accurate post-expansion plasma diameter and temperature. These results, therefore, suggest the discontinuation of TSM in favor of iTSM to determine the post-breakdown state. Moreover, there seems to be no reason to keep utilizing TSM if equilibrium plasma properties were already coded for the ensuing steps of the ignition model, as is the case of [Lucchini et al. \(2013\)](#), [Cornolti \(2015\)](#), [Zhu et al. \(2016\)](#) and [Sforza et al. \(2017\)](#).

2.3 0DTM

Rather than splitting the process of energy addition and channel expansion, one could try to determine the time of pressure equalization via dimensional reasoning, as done by [Meyer and Wimmer \(2018\)](#). Using the well known ([Plooster, 1970](#)) temporal ($t_0 = R_0/a_0$) and spatial ($R_0 = [E_{bd}/(d_g b \gamma p_0)]^{1/2}$) scales, where a_0 is the speed of sound and $b = 3.85$ is a constant

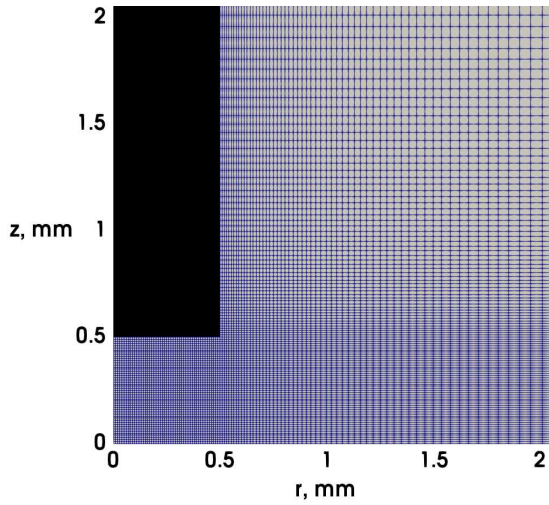


Figure 3: Partial visualization of the meshed domain.

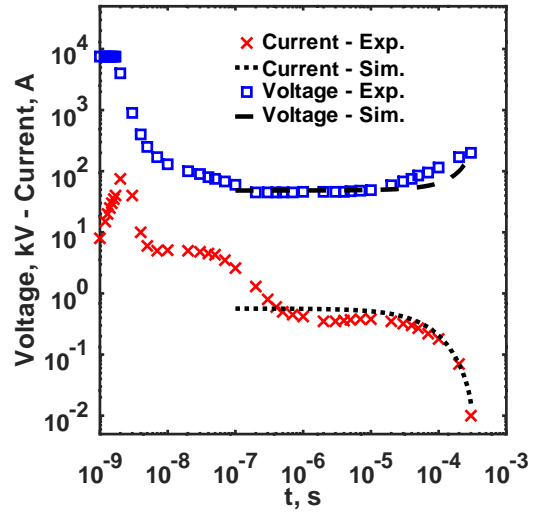


Figure 4: Voltage and current of the CDI system as a function of time. Symbols: Maly (1984). Lines: equivalent circuit calculations. Pressure: 2 bar. Temperature: 300 K. Spark gap size: 1 mm.

(Meyer and Wimmer, 2018), they arrived to the same result obtained by Ko et al. (1991), i.e. $\tau = t/t_0 = 1.5$ as the nondimensional time when pressure equalizes the chamber value. Then, the one-dimensional results obtained by Plooster (1970) for a cylindrical blast wave were employed to set the plasma boundary at $\lambda = r_i/R_0 = 0.5$, defined as the radius corresponding to a nondimensional density $\rho/\rho_0 \approx 0.9$, where ρ_0 is the unperturbed density. Once the boundary is known, an application of the first law of thermodynamics allows to determine the expanded kernel average enthalpy \bar{h}_i (and temperature):

$$(\bar{h}_i - \bar{h}_u)\bar{\rho}_i V_i = \eta_{bd} E_{bd} \quad (7)$$

where h_u is the unburned enthalpy and η_{bd} is the breakdown efficiency. Two major drawbacks of this methodology are the assumption of a cylindrical kernel and the presumed η_{bd} . The authors adopted $\eta_{bd} = 0.82$ for their calculations, so this number will also be taken as reference here.

3 CONSERVATION EQUATIONS AND NUMERICAL PROCEDURE

Mass, momentum and specific enthalpy conservation for a compressible laminar flow may be written as follows (Poinsot and Veynante, 2012):

$$\frac{\partial \rho}{\partial t} + \frac{\partial \rho u_i}{\partial x_i} = 0 \quad (8)$$

$$\frac{\partial \rho u_j}{\partial t} + \frac{\partial \rho u_i u_j}{\partial x_i} + \frac{\partial p}{\partial x_j} = \frac{\partial}{\partial x_i} \left[\mu \left(\frac{\partial u_i}{\partial x_j} + \frac{\partial u_j}{\partial x_i} - \frac{2}{3} \delta_{ij} \frac{\partial u_k}{\partial x_k} \right) \right], \quad j = 1, 2, 3 \quad (9)$$

$$\frac{\partial \rho h}{\partial t} + \frac{\partial \rho u_i h}{\partial x_i} + \frac{\partial q_i}{\partial x_i} = \frac{\partial p}{\partial t} - \rho \frac{DK}{Dt} + \dot{q}_v \quad (10)$$

where ρ is the density, u_i is the i-th velocity component, p is the pressure, K is the mean kinetic energy, μ is the dynamic viscosity, h is the specific enthalpy, q_i is the heat flux, \dot{q}_v is the energy

source term and δ_{ij} is the Kronecker delta tensor. In Eq. (10) the viscosity dissipation term was neglected. The fluid is modelled as a thermal air plasma, whose properties were taken from [D'angola et al. \(2008\)](#).

The system of equations was implemented in OpenFOAM[®], which employs the Finite Volume Method (FVM) with a cell-centered collocated variable arrangement. The solver uses a combination of the SIMPLE (Semi-Implicit Method for Pressure-Linked Equations, [Patankar \(1980\)](#)) and PISO (Pressure-Implicit with Splitting Operators, [Issa \(1986\)](#)) algorithms. All discretization schemes match those of a previous work ([Aranciaga et al., 2019](#)), and for the sake of brevity will not be repeated here.

4 CASES DESCRIPTION

The geometric configuration corresponds to two opposed, 1 mm diameter cylindrical electrodes, with a spark gap size $d_g = 1$ mm. The initial air temperature and pressure are 300 K and 1 bar, respectively. Two very different electrical discharges are to be simulated (c.f. [Maly \(1984\)](#)):

- Case A: a 3 mJ, 100 μ s capacitor discharge ignition (CDI)
- Case B: a 30 mJ, 60 ns breakdown ignition.

Figure 3 depicts part of the computational domain and the mesh structure. Taking advantage of the symmetry of the electrodes geometry and their relative position, half of the domain is selected in the axial coordinate z , and a wedge of it is solved in the tangential direction. The maximum radius and z are both set equal to 25 mm, in order to be able to run a sufficient amount of time (50 μ s) without giving time to the pressure wave to reflect at the edges and propagate back to the kernel region. Therefore, zero-gradient for all of the fields were used as boundary conditions for $z = z_{max}$ and $r = r_{max}$. Regarding the electrode walls, a no-slip condition for the velocity field was adopted, a null gradient for the pressure field and a fixed temperature $T = 300$ K for the energy equation, in order to take into account heat conduction losses in a simplified way. The back and front faces are of the wedge type, and at $z = 0$ a symmetry plane exists. Radiation losses are not included, given that [Ekici et al. \(2007\)](#) showed them to be around one order of magnitude lower than conduction losses. The minimum cell size is 10 μ m, uniformly distributed in the spark gap region, and a grading of 3% between adjacent cells is applied in both radial and axial coordinates outside of it, yielding 723 μ m as the maximum cell size for the farthest cell from the origin. The time step size was variable, such that the maximum localized Courant Number would not exceed 0.2. Both the time step and mesh refinement were selected according to a convergence analysis not shown in this work for conciseness reasons. Initially, time steps are extremely small ($\approx 10^{-11}$ s) and only the spark gap region perceives the discharge perturbation. Thus, the simulation is run on a more refined reduced mesh (cell sizes between 2.8 and 9.2 μ m) covering this region, until the pressure wave is about to touch the border $r = r_{electrode}$, from which all fields are mapped to the main domain and the simulation goes on. The initial condition is chosen to be the output of the first stage of iTSM (isochoric breakdown energy input). This is substantiated by some runs where this alternative was compared to a constant power source with varying radii and durations and the differences encountered long after the discharge ($\tau \approx 0.7$) were quite small. Similar observations were reported by [Colin et al. \(2019\)](#). The breakdown energy for case A is $E_{bd,A} \approx 0.3$ mJ, while that for case B is $E_{bd,B,reported} = 30$ mJ. Low breakdown energies are associated with very high deposition efficiencies (close to unity) according to [Maly \(1984\)](#). On the contrary, very high

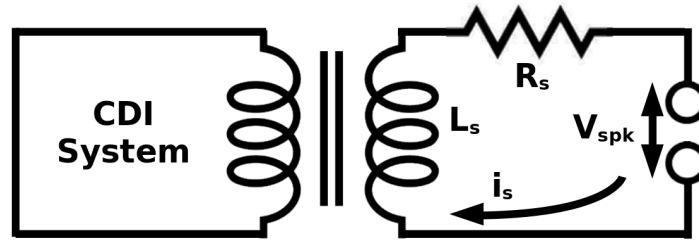


Figure 5: Electrical equivalent circuit diagram.

breakdown energies deviate considerably from those ideal values. For standard conditions, a breakdown ignition device with 30 mJ discharged energy across a 2 mm gap would transfer about 15 mJ to the gas (Maly, 1984), and this is the value to be used in this work. For 60000 K plasma channels, these energies yield a radius of 26.9 μm for case A and 190 μm for case B. The latter does not require any additional energy input, but the former (CDI system) does. For that purpose, an equivalent electrical circuit is employed (Fig. 5) where the energy stored in a capacitor is discharged through a transformer elevating the voltage to produce the breakdown in the spark gap. Energy stored in the secondary inductance L_s , $E_s = 0.5L_s i_s^2$ (i_s being the secondary current) is then transferred to the spark gap, losing a fraction of it through joule heating in the secondary resistance R_s , according to the following equation:

$$\frac{\partial}{\partial t}(0.5L_s i_s^2) = -R_s i_s^2(t) - V_{spk}(t) i_s(t) \quad (11)$$

The spark gap voltage V_{spk} is the sum of the anode and cathode falls, and the positive gas column voltage V_{gc} . Both fall voltages are obtained from Sforza et al. (2017), and the power consumed by them is deemed as completely lost to the electrodes. For V_{gc} a correlation proposed by Kim and Anderson (1995) is adopted, which accounts for pressure, electric current and spark length effects. The adjustment coefficients correspond to the arc mode due to the voltage/current characteristics of this mode of energy transfer. The parameters L_s and R_s are calibrated against measured current and voltage evolutions (Maly, 1984) at high pressure (see Fig. 4). This curves represent twice the pressure magnitude than the simulated cases. Nonetheless, variations when halving the pressure for agreement with the simulations are quite moderate. For each time step the source of energy in Eq. (10) is computed as the electric power transmitted to the positive gas column, i.e. $Q_v = \int \dot{q}_v dV = V_{gc}(t) i_s(t)$, where the domain of integration is assumed to be a cylinder extending across the spark gap and 0.4 mm radius, in agreement with Colin et al. (2019).

5 COMPUTATIONAL RESULTS AND DISCUSSION

Peak temperatures are monitored during the first 50 μs after discharge and compared in Fig. 6 to the corresponding reported values (Maly, 1984). Considering the uncertainties and simplifications the overall code performance is rather satisfactory. Deviations for $t < 10^{-7}$ s might well be attributable to the adoption of the first stage of iTSM as initial condition. The assertion of its adequacy stated in Section 4 applies to times sufficiently far from the discharge. The discrepancy of the breakdown curves between $10^{-7} < t < 10^{-5}$ s could be due to a different flow field originated from an erroneous electrode geometry, leading to distinct convection cooling rates. Since the flow field is mainly pressure-driven in this phase, the CDI case was more immune to this defect, given its lower blast wave energy. It is interesting at this point to compute the output

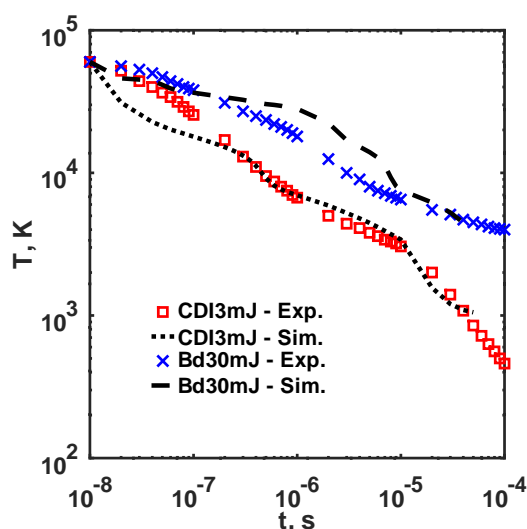


Figure 6: Peak temperature vs. time for the two ignition systems: CDI and breakdown. Symbols: Maly (1984). Lines: equivalent circuit calculations.

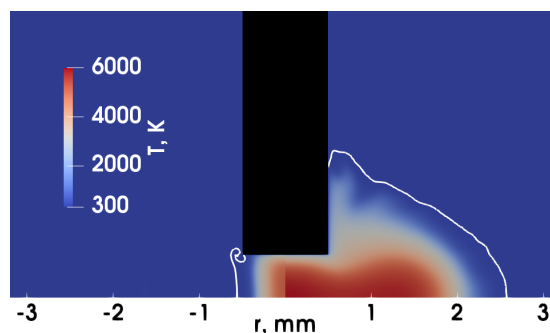


Figure 7: Temperature fields for the tested cases. Left: case A. Right: case B. White lines represent isotherms $T = 330$ K, corresponding to $\rho/\rho_0 \approx 0.9$.

temperatures and channel diameters for both iTSM and ODTM. The latter is clearly associated with a specific instant of time ($\tau = 1.5$), while the former is not. One could relate it to the same value of τ , but focusing only on pressure decreasing to values previous to the discharge (as it is the basis of the model), this would be accomplished around $\tau \approx 0.3$. Between $0.3 < \tau < 1.5$, flow effects do not seem negligible, therefore becoming imperative to consider them in the model afterwards. Since this is normally not the case¹, $\tau = 1.5$ will also be selected for iTSM. This nondimensional time translates into $t = 3.22 \mu\text{s}$ and $t = 22.8 \mu\text{s}$ for cases A and B, respectively. Table 1 summarizes the results. The computationally computed plasma temperature T_i corresponds to the volume average delimited by the isotherm $T = 330$ K. Temperatures predicted by iTSM are one order of magnitude higher than the simulated results, as already pointed out by Meyer and Wimmer (2018). Their model yields much closer temperatures, although deviations are still significant. This may be due to an inaccurate breakdown efficiency (its lack of knowledge is one of the model's weak points). Errors in diameter predictions are more modest for both models, especially for the highest energy case. For the simulation, d_i in Table 1 results from evaluating the isotherm $T = 330$ K ($\rho/\rho_0 \approx 0.9$) along the symmetry radial axis. As Fig. 7 depicts, the low energy case resembles rather well a cylinder, though the high energy case is far from such simple shape. Moreover, although the pressure is almost uniform for $\tau > 1.5$, convective effects keep shaping the kernel into a quasi-torus afterwards, so that becoming essential that future ignition models take into account this departure from the simple cylindrical volume. It is true that typical ignition devices either do not work with such high discharge energies, or do so in a high pressure environment (as in spark-ignition engines) resulting in reduced kernel dimensions, where the cylindrical volume is more appropriate. In any case, specifications of model limitations are currently lacking. It is believed that they should be clearly stated for a more reliable use of them.

¹Most models utilizing TSM/iTSM as initial conditions continue by solving thermal diffusion equations, completely neglecting convective effects.

	T_i , K (case A)	d_i , mm (case A)	T_i , K (case B)	d_i , mm (case B)
Simulation	1600	1.10	2550	5.12
iTSM	35100	0.682	35100	4.82
ODTM	4385	0.746	4503	5.28

Table 1: Plasma channel temperature and diameter for different models.

6 CONCLUSIONS

Initialization strategies of typical ignition models have been analyzed, initially through a comparison between the ideal gas (TSM) and real gas (iTSM) versions and lastly against computational results. A more novel approach (ODTM) was also considered, which claimed to yield more physical kernel temperature values compared to the former methodologies. The first noteworthy observation is that the ideal gas assumption, TSM (which is the course adopted in many models) is a very poor approximation against the real gas version iTSM, since it is not able to simultaneously predict the expanded channel temperature and diameter. In spite of its practicality, its improved version iTSM is still quite simple to implement. Therefore, there would be no reason to continue employing TSM. On the other hand, the claim of Meyer and Wimmer (2018) about the unrealistically high expanded channel temperature is also confirmed in this work, therefore suggesting their model (ODTM) as an improved means of initializing a combustion simulation. Nonetheless, a more rigorous method should be developed which accounts with kernel shape distortion and energy losses in a more accurate way.

REFERENCES

- Aranciaga J., López E., and Nigro N. Modelling of ignition process for premixed combustion in a constant volume bomb. In *Mecánica Computacional Vol XXXVII*, pages 983–992. Santa Fe, Argentina, 2019.
- Bane S.P., Ziegler J.L., and Shepherd J.E. Investigation of the effect of electrode geometry on spark ignition. *Combust. Flame*, 162(2):462–469, 2015. ISSN 0010-2180.
- Colin O., Ritter M., Lacour C., Truffin K., Mouriaux S., Stepanyan S., Lecordier B., and Vervisch P. DNS and LES of spark ignition with an automotive coil. *Proceedings of the Combustion Institute*, 37(4):4875–4883, 2019. doi:10.1016/j.proci.2018.08.021.
- Colin O. and Truffin K. A spark ignition model for large eddy simulation based on an FSD transport equation (ISSIM-LES). *Proc. Combust. Inst.*, 33:3097–3104, 2011.
- Cornolti L. *CFD modelling of turbulent premixed combustion in spark ignition engines*. Ph.D. thesis, Politecnico di Milano, 2015.
- D’angola A., Colonna G., Gorse C., and Capitelli M. Thermodynamic and transport properties in equilibrium air plasmas in a wide pressure and temperature range. *European Physical Journal D*, 46:129–150, 2008.
- Ekici O., Ezekoye O., Hall M., and Matthews R. Thermal and flow fields modeling of fast spark discharges in air. *Journal of Fluids Engineering*, 129, 2007.
- Essmann S., Markus D., and Maas U. Investigation of the spark channel of electrical discharges near the minimum ignition energy. *Plasma Phys. Technol.*, 3:116 – 121, 2016.
- Falfari S. and Bianchi G.M. Development of an ignition model for S.I. engines simulation. In *SAE Technical Paper*. SAE International, 2007.
- Forte C., Bianchi G.M., and Corti E. Validation of a lagrangian ignition model in SI engine simulations. In *Internal Combustion Engine Division (Publication) ICE*. American Society

- of Mechanical Engineers, 2010.
- Herweg R. and Maly R.R. A fundamental model for flame kernel formation in S.I. engines. *SAE Transactions*, 101:1947–1976, 1992. ISSN 0096736X, 25771531.
- Issa R. Solution of the implicitly discretised fluid flow equations by operator-splitting. *Journal of Computational Physics*, 62(1):40–65, 1986.
- Kim J. and Anderson R.W. Spark anemometry of bulk gas velocity at the plug gap of a firing engine. *SAE Transactions*, 104:2256–2266, 1995.
- Ko Y., Arpaci V., and Anderson R. Spark ignition of propane-air mixtures near the minimum ignition energy: Part II. A model development. *Combust. Flame*, 83(1):88 – 105, 1991. ISSN 0010-2180.
- Lucchini T., Cornolti L., Montenegro G., D’Errico G., Fiocco M., Teraji A., and Shiraishi T. A comprehensive model to predict the initial stage of combustion in SI engines. *SAE Technical Paper*, 2013-01-1087, 2013.
- Maly R. *Fuel Economy in Road Vehicles Powered by Spark Ignition Engines*. (J. C. Hilliard and G. S. Springer, eds.), Plenum Press, 1984. ISBN 9780306414381.
- Meyer G. and Wimmer A. A thermodynamic model for the plasma kernel volume and temperature resulting from spark discharge at high pressures. *J Therm Anal Calorim*, 133:1195 – 1205, 2018.
- Nakaya S., Hatori K., Tsue M., Kono M., Segawa D., and Kadota T. Numerical analysis on flame kernel in spark ignition methane/air mixtures. *Journal of Propulsion and Power*, 27(2):363–370, 2011.
- Patankar S.V. *Numerical Heat Transfer and Fluid Flow*. Taylor & Francis, 1980.
- Plooster M.N. Shock waves from line sources. Numerical solutions and experimental measurements. *The Physics of Fluids*, 13:2665–2675, 1970.
- Poinsot T. and Veynante D. *Theoretical and Numerical Combustion*. Poinsot T. and Veynante D., 3 edition, 2012.
- Refael S. and Sher E. A theoretical study of the ignition of a reactive medium by means of an electrical discharge. *Combust. Flame*, 59(1):17–30, 1985. ISSN 0010-2180.
- Sforza L., Lucchini T., Onorati A., Zhu X., and Lee S.Y. Modeling ignition and premixed combustion including flame stretch effects. In *SAE Technical Paper*. SAE International, 2017.
- Shen H., Hinze P.C., and Heywood J.B. A model for flame initiation and early development in SI engine and its application to cycle-to-cycle variations. In *SAE Technical Paper*. SAE International, 1994.
- Sher E., Ben-Ya’Ish J., and Kravchik T. On the birth of spark channels. *Combust. Flame*, 89(2):186–194, 1992. ISSN 0010-2180.
- Song J. and Sunwoo M. A modeling and experimental study of initial flame kernel development and propagation in SI engines. In *SAE Technical Paper*. SAE International, 2000.
- Tan Z. and Reitz R.D. An ignition and combustion model based on the level-set method for spark ignition engine multidimensional modeling. *Combustion and Flame*, 145(1):1–15, 2006. ISSN 0010-2180. doi:<https://doi.org/10.1016/j.combustflame.2005.12.007>.
- Zhu X., Sforza L., Ranadive T., Lee S.Y., Naber J., Lucchini T., Onorati A., Anbarasu M., and Zeng Y. Experimental and numerical study of flame kernel formation processes of propane-air mixture in a pressurized combustion vessel. *SAE International Journal of Engines*, 9, 2016.